Journal of Catalysis **191,** 200–217 (2000)
doi:10.1006/jcat.1999.2789, available online at http://www.idealibrary.com on IDEAL®

Study of the Hydrolysis of Acetonitrile Using Different Brønsted Acid Models: Zeolite-Type and $HCl(H_2O)_x$ Clusters

Luis A. M. M. Barbosa[1] and Rutger A. van Santen

Schuit Institute of Catalysis, Laboratory of Inorganic Chemistry and Catalysis, Eindhoven University of Technology, P.O. Box 513, 5600 MB Eindhoven, The Netherlands

Received September 14, 1999; revised December 13, 1999; accepted December 13, 1999

The hydrolysis of acetonitrile has been studied theoretically by different *ab initio* methods (RHF, DFT, and MP2). Two Brønsted acid catalysts have been compared: zeolite and $HCl(H_2O)_{x=2,1}$ clusters. Some interesting analogies have been found for the reaction path catalyzed by these different acids, especially in the hydration transition state. The size and the configuration of a zeolite cluster model have an important influence on predicting the reaction mechanism. The van der Waals interactions also play an important role in this reaction. Due to these interactions, oxygen atoms of the zeolite cavity can stabilize charged species as N- and O-protonated acetamide configurations. For the zeolite catalyst, the rate-limiting step of the overall reaction is the hydration of acetonitrile. On the other hand, in the hydrochloric acid catalysis, the rate-limiting step is either the hydration or the isomerization step. Acetamide appears to be the most stable species adsorbed on zeolite and it is responsible for poisoning the reaction.

Key Words: ab initio; **hydrolysis; Brønsted acid site; zeolites; water molecule.**

1. INTRODUCTION

Lately, increasingly stringent environment constraints have led to a significant effort in new industrial routes and catalyst design and application. However, current industrial processes for organic acid synthesis are known to be environmentally unfriendly. The majority of these processes is based on the oxidation of alkylaromatic compounds as toluene, ethylbenzene, and xylenes (1). One example is the production of terephthalic acid, which ranks about 25th in tonnage of all chemicals and 10th of all organic compounds together with its dimethyl ester (2).

A less explored alternative for the production of such acids is the hydrolysis of nitriles, which is a well-established catalytic procedure in acidic and basic media and has been continuously used in many organic chemistry lab classes (3). Another interesting point is that nitriles appear in industrial-waste stream (4); therefore it is necessary to develop new processes to solve this problem.

The nitrile hydrolysis reaction proceeds via a succession of four steps: protonation of nitrile, water nucleophilic attack, protonation of amide (product of the first hydration), and finally second water nucleophilic attack (3). Thus, the complete process requires two water molecules as reactants (Scheme 1).

Different catalysts have been employed to promote this reaction. Manganese oxide (5), unactivated alumina (6), high-temperature water (4), Pd(II) (7) and dirhenium complexes (8), hydroxylated zirconium dioxide (9), copper-nickel alloys (10), hydrotalcite-like materials (11), ionic copper, and copper oxide (see a review on hydration/hydrolysis reaction (12)) are few examples.

Even enzymatic hydrolysis has been getting more and more attention in this particular field due its very high stereoselectivity and use in a wide range of substrates (13). This has led to a development of a large-scale industrial process for production of acrylamide from acrylonitrile (13c). Unfortunately, enzymatic processes are not economically competitive in most of the cases.

A new class of Brønsted acid catalysts, protonic zeolites, has been recently developed, based on so-called first generation Brønsted acids (aqueous solution of hydrochloric and sulfuric acid (14)), and employed for hydrolysis of diverse molecules (15). Interestingly, the nitrile hydrolysis has been studied as a side reaction of the formation of ethyl esters from aromatic nitriles on different zeolites (15a).

The first Brønsted acid catalyst studied here is protonic zeolite. This catalyst is modeled by "3T", "4T", and "5T" clusters. Several other zeolite-catalyzed reactions have been successfully studied theoretically. The activation of C–H and C–C bonds (16), the study of methanol reactions in zeolites (17), and interaction studies between the Brønsted acid sites and chemical species (18) are a few examples.

The other Brønsted acid catalyst is hydrochloric acid. This catalyst is modeled by the $HCl(H_2O)_{x=2,1}$ cluster, the so-called "homogeneous model." A similar homogeneous

[1] Fax: +31 40 245 5054. E-mail: tgaklb@chem.tue.nl.

0021-9517/00 $35.00

SCHEME 1. Hydrolysis of acetonitrile.

approach has also been used before in theoretical studies of hydrolysis of isocyanates (19), of β-Lactams (20), and of parent carbodiimides (21). In this model, one of the water molecules is a nucleophile, while the other represents a solvent. The second water molecule also acts as a basic molecule, which is a homogeneous analogue of basic oxygen atoms of the zeolite. This methodology is very useful in understanding and comparing the reaction mechanisms in the zeolite cluster model.

Our aim is to compare these two different Brønsted acid catalysts—protonic zeolites and hydrochloric acid in acetonitrile hydrolysis.

Acetonitrile (An) has been chosen as a model for simplicity (small nitrile molecule). Its size and structure are evocative of typical reactants in zeolitic-catalyzed reactions (17, 22). Furthermore, acetonitrile has also been widely used to probe the Lewis and Brønsted acidity of zeolites (18a, 18e, 22d, 23).

The paper is organized as follows: first, adsorption of acetonitrile is studied and then the hydrolysis mechanism is considered. For a better understanding, the reaction is divided into three distinct steps: hydration, isomerization (tautomerization), and desorption of product (see Scheme 2). Water ancillary and product poisoning effects are discussed along all reaction paths.

2. METHODS

In this work, different cluster fragments were used to model the Brønsted acid site: 3T ($H_3SiOHAl(OH)_2OSiH_3$), 4T ($H_3SiOHAl(OSiH_3)_2OH$), 5T ("4Tring" plus $OSiH_3$ group) for zeolite and $HCl(H_2O)_x$, in which x changes from 1 to 2. In the zeolite models, the Al center has two or three adjacent oxygen basic atoms, which are necessary for hydrogen bonding with OH and NH groups (24).

The 3T model was used to study the adsorption of acetonitrile and acetamide. The 4T model is shown to be needed in the hydration mechanism study, even though the 3T cluster could also be used with some configuration changes. For the isomerization study, larger clusters, which have two adjacent acid sites, were necessary. Later more details about this extra site requirement are provided.

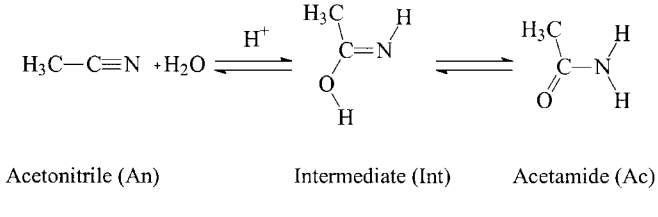

SCHEME 2. First step of the hydrolysis.

H termination of the Si group has been chosen instead of OH termination to avoid problems such as intramolecular hydrogen bond formation, which results in the creation of a nonacceptable model (25). Clusters provide qualitatively interesting results with activation energies typically 10 kJ/mol higher than those for extrapolated bulk zeolite reactions. The use of such clusters has been extensively discussed elsewhere (24, 26).

All the calculations have been performed using two different types of basis sets with polarization functions: D95 Dunning/Huzinaga full double $-\zeta$ (27) (for Cl, Si, Al, C, N, H) and 6-311G (for the O). For studies of methanol and ammonia in zeolites, such combination of double and triple $-\zeta$ plus polarization function type has been successfully employed with 3T or bigger models (28). Large basis sets, at least double $-\zeta$ type, have been shown to be necessary for good accuracy in energy and physical properties (29).

Restricted Hartree Fock (RHF), density functional theory (DFT), and second-order Møller-Plesset perturbation theory (MP2) have been used in this study. RHF calculations were used to save computer time and to obtain initial guesses for the other calculations. MP2 is used to correct the RHF geometry and energy in our systems for small systems. For small zeolite clusters (3T and 4T), MP2 was used only to correct the RHF energy (single-point calculations). Neither MP2//RHF nor RHF was used for the 5T model.

DFT calculations were performed because they include some electron correlation and it scales much better than the previous MP2 method (29). The hybrid B3LYP functional was used, which gives acceptable values for molecular energies and geometries (30, 31). A comparison of all three methods is provided in this paper.

The results were obtained with Gaussian94 (32) and 92 (33) packages. The DFT calculations using the 92 version were performed using Int=FineGrid keyword (which is a default on the 94 version) (34) to avoid numerical inaccuracies in the energy and gradients calculations. The hybrid B3LYP functional was used in our work as implemented in Gaussian94 (32) or 92 (33) codes.

For RHF and DFT calculations, all the stationary points (transition states and geometry minima) were verified by frequency calculations. These tests produce no imaginary frequencies for local minimum and one imaginary frequency for transition states (first-order saddle points) (35). The computation of Hessian matrix within MP2 framework requires large resources; therefore the DFT geometry and Hessian are used as initial guesses, which are updated according to MP2 forces.

RHF and DFT energies were also corrected using zero-point energy (ZPE). The basis set superposition error (BSSE) was verified for DFT and MP2 ("homogeneous model") using the counterpoise method (36). Although our

calculations involve more than two molecules, the N-body counterpoise method (37) was not applied completely. For most of the cases studied here, such procedures become very expensive. For example, 22 calculations and 125 calculations are required for the 3-body system and for the 4-body system, respectively. Instead, the 3-body method was applied to one system (4T model plus acetonitrile plus water). To complement the BSSE investigation, the 2-body method was applied in five different cases, such as HCl plus water, acetonitrile plus water, acetonitrile plus HCl, 4T model plus acetamide, and 5T model plus intermediate. On average, the BSSE contents (in percentage) for these interaction energies were 21.2 and 27.9, respectively, for DFT and MP2 (only for the binary systems of the homogeneous model). These values are in agreement with recent studies of BSSE for H-bonded complexes (38). Even though these values are not negligible, the BSSE was not corrected but simply verified in our results (see also recommendations in previous specific studies on this subject (36, 37)).

No symmetry constraints have been used for most of the configurations studied (all exceptions are described in the text). For deprotonation energy calculations the 5T model has been used with some constraints to prevent unrealistic configurations, which were found in the optimization of the full-relaxed 5T models. Since MP2, RHF geometries are quite similar to DFT in most of the cases, the latter geometries are shown in all figures and tables. RHF and MP2 energies are shown only when it is necessary.

3. RESULTS AND DISCUSSION

3.1. Adsorption of Acetonitrile

Figure 1a shows the computed acetonitrile adsorption complex using the 3T model. This configuration indicates that An forms a hydrogen bond with the Brønsted site through a nitrogen lone pair. This optimized structure is similar to that previously found by Hall *et al.* (23) and Florian and Kubelkova (22d). The angles O(3)–H(8)–N and C(18)–N–H(8) are less than 180°. In (23) the angle C(18)–N–H(8) was found to be 161.3° and in (22d) it is equal to 175.6°, while our results (see Table 1) show values of 172.9 and 162.8° for the DFT and RHF methods, respectively. The homologous angle in the $HCl(H_2O)_2$ model is C(9)–N–H(6) and its value is 161.4 and 163.3° for the DFT and RHF methods, respectively, which is in a good agreement with the previous values.

The distance between the Brønsted site and acetonitrile is 1.75 and 1.73 Å (for the DFT method) for the zeolite and the $HCl(H_2O)_2$ models, respectively. One can note that acetonitrile has a similar position for both Brønsted acid catalyst models studied. All these results are also in agreement with the rules developed for gas-phase hydrogen-bonded dimers (39), where it has been found that the nonbonding pair interacts with acidic protons.

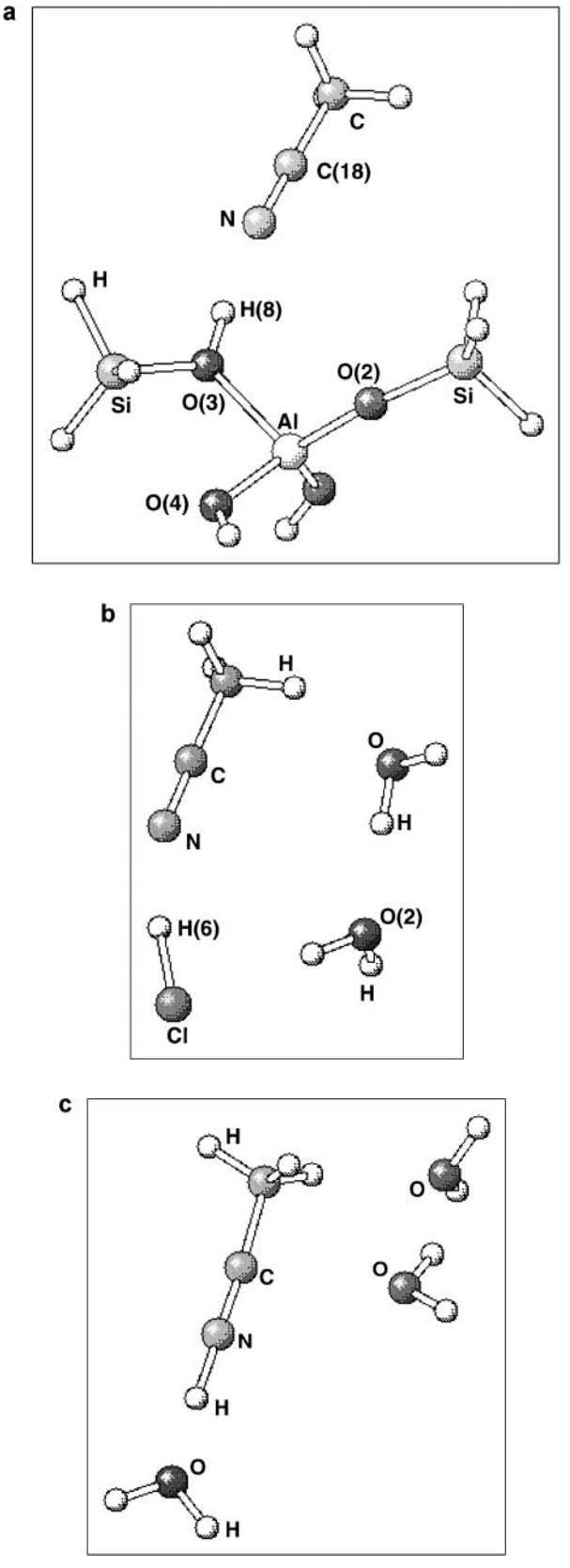

FIG. 1. (a) Acetonitrile and zeolite model. (b) Acetonitrile and $HCl(H_2O)$ model. (c) Acetonitrile and $H_3O^+(H_2O)$ model.

TABLE 1

DFT Optimized Geometries for Various Systems (DFT/B3LYP)

	$HCl(H_2O)_x$ model		Zeolite model		
	Cluster and acetonitrile	Cluster (3T)	Cluster and acetonitrile (3T)	Cluster and acetamide (4T) Ac1	Ac2
Al–O(3)	—	1.94	1.92	—	—
Si–O(2)–Al	—	156.4°	153.7°	—	—
Si–O(3)–Al	—	114.9°	118.9°	—	—
O–H(8)	—	0.96	0.99	—	—
N–H(8)	—	—	1.73	—	—
O(3)–H(8)–N	—	—	174.1°{168.4°}	—	—
C(18)–N–H(8)	—	—	172.9°{162.8°}	—	—
H(8)–O(3)–Si	—	117.6°	—	—	—
H(8)–O(3)–Al	—	127.4°	—	—	—
Si–O(3)–Al–O(4)	—	6.25°{6.87°}	—	—	—
O(24)–O(3)	—	—	—	—	2.52
N–O(2)	—	—	—	2.93	2.85
N–O(3)	—	—	—	2.71	—
N–H(6)	1.75	—	—	—	—
C(9)–N–H(6)	161.4°{163.3°}	—	—	—	—

Note. All distances are in angstroms (Å) and angles in degrees. {RHF} values.

The cluster model geometry is also comparable with earlier reported results. For instance, the distances Al–O(3) and O(3)–H(8) were calculated to be 1.98 and 0.98 Å by Gale (24), 1.94 and 0.95 Å by Sauer (28a), and 1.94 and 0.96 Å in this work for the DFT method. Following the previous comparison, the model angles also behave similarly, H(8)–O(3)–Si and H(8)–O(3)–Al are 117.5 and 107.6° in (24) or 120.0 and 132.0° in (28a) and 117.6° and 127.4° in this work, respectively (see Table 1). The average value for the angles between the T atoms, Si–O(3)–Al and Si–O(2)–Al, is 135.7° in this work. These values are in good agreement with the experimental values found for ZSM-5, which range from 147.1 to 158.8° in a monoclinic framework and from 144.9 to 175.9° in an orthorhombic framework (40).

The spatial positions of Si, O(3), Al, and OH groups show an interesting phenomenon. The dihedral angle between Si, O(3), Al, and O(4) in our studies is 6.25° for DFT (see Table 1) and 6.87° for RHF, which means that these atoms are almost in the same plane. This distortion has not been found in a real zeolite frame; thus it might be a source of important differences.

To verify a possible influence on our results, calculations of acetonitrile adsorption and deprotonation energy were also performed using some geometric constraints in the cluster model. The first idea is to fix the position of the Al atom, nonbridging oxygen, and SiH_3 groups as found in faujasite. The other idea is to fix only the nonbridging oxygen and SiH_3 groups.

The resulting deprotonation energies for all models (with or without constraints) can be found in Table 2. Our results do not significantly change and are in a good agreement with previously calculated and experimental values (41). Therefore, the geometry differences found in our model have only a small influence on the results.

One remark should be made about the value of the adsorption energies found in this study (using the full optimized 3T cluster), which are 51.9 and 54.7 kJ for DFT and MP2//RHF calculations, respectively. Comparing these values to the experimental result of 80 kJ/mol (for HY) (42), one concludes that our zeolite model does not represent completely the real zeolite environment for acetonitrile adsorption. Cluster models do not contain any stabilizing effects that result from the van der Waals interactions of acetonitrile with zeolite cavity oxygen atoms. The energy difference between cluster calculations and experiment agrees with data on the adsorption energy of acetonitrile in siliceous zeolites, which show values between 30 kJ/mol (43) and 60 kJ/mol (44).

The interaction energy between acetonitrile and HCl (without water molecules) has also been calculated to be 22.4 kJ/mol for the DFT method. This value is around half that previously found for the zeolite model. However, when two water molecules are added to the model, this energy increases to the value of 85.3 kJ/mol, which is similar to the experimental value for the zeolite. This water addition strengthens the acidity of the HCl cluster model in the gas phase.

In all of our calculations acetonitrile is not protonated by the zeolite cluster. Even when this protonated geometric configuration was employed as the initial structure, the

TABLE 2

Deprotonation and Adsorpion Energies (DFT/B3LYP) for Various Methods and Models (kJ/mol)

Model used	Deprotonation energy	Acetonitrile adsorption energy	Acetamide adsorption energy		
			Ac1	Ac2	Ac3
3T—2-dimensional	1301.4	−47.5 {−42.6} [−54.7]	−44.4 {−26.7} [−53.9]	−85.4 {−61.2} [−97.3]	−14.1 {+30.6} [−24.2]
3T—2-dimensional with constraints (Al, SiH_3, OH)	1268.6	−59.8			
3T—2-dimensional with constraints (SiH_3, OH)	1280.6	−51.9			
3T—3-dimensional	1331.0	—			
4T	1287.3	−49.9	−44.9 {−26.2} [−56.3]	−90.2 {−68.3} [−94.7]	−11.2 {+37.1} [−19.9]
5T with constraints	1304.2				
Experimental values for zeolites	1139–1204 (41a)	80 (42)			
$HCl(H_2O)_{x=2,1,0}$ model	—	22.4, $x=0$ 85.3, $x=2$			

Note. {RHF} value and [MP2//RHF] value.

proton migrates back to the cluster. This agrees with the interpretation of infrared spectra studies of acetonitrile adsorbed on zeolites (18a,e, 22d) and has also been observed before in different types of calculations (23, 45).

Zeolites also cannot protonate *p*-nitrotoluene and *p*-fluornitrobenzene (30). These molecules are considered bases with H_0 at the border of super-acidity, indicating that zeolites do not have a super-acidity character. This result was also confirmed by the NMR study of carbenium formation (46), where zeolites appeared not to be stronger than 80% sulfuric acid solution. A similar result has been found for hydrochloric acid, because our model is still far from the real state of hydrochloric acid in solution (see Fig. 1b). When H_3O^+ is used as a proton donor (47a), acetonitrile indeed becomes protonated, see Fig. 1c. H_3O^+ is a better proton donor than HCl in the gas phase. Similar proton strength dependency was also verified by Kazansky *et al.* (47b,c).

3.2. Hydration Step

Our first attempt to calculate the reaction path using the 3T model has failed. The so-called "2-dimensional model" has only two adjacent oxygen atoms (see Fig. 1a), which do not seem to be enough to accommodate both reactant molecules: An and water. However, this problem was overcome when the 3T model with a different geometry was used. This new configuration, so-called "3-dimensional model," has three oxygen sites (Fig. 2a). The drawback of this model is the existence of two nonequivalent oxygen sites: O(4) and O(2)/O(3). To check the influence of this inequality, a 4T model, which is the previous model with $OSiH_3$ group replacing one OH group, was also used (see Fig. 2b).

Comparing these two models, one can see that the activation energy values and final geometries of the transition states (Ts1–3T and Ts1-4T) for the hydration step are in good agreement (Table 3 and Figs. 3a and 3b). However, the inequality of oxygen atoms O(4) and O(3) in 3T cluster influences the reaction energy, since different Brønsted sites are formed during the reaction (see Table 3).

Similar transition states have been found for both zeolite and $HCl(H_2O)_2$ cluster models, compare Figs. 3a,b, and c. The C–O distance, represented by C(18)–O(23) and C(9)–O(3), decreases to 1.82 and 1.92 Å for these clusters, respectively (see Table 4). N–C–O angle, represented by N–C(18)–O(23) and N–C(9)–O(3), becomes closer to the final result: 118.9 and 113.8 Å, respectively. These geometric values represent the nucleophilic attack and the formation of a C–O single bond.

Hall *et al.* (23) proposed transfer of the proton from zeolite to An with its bending, where the C hybridization changes from *sp* to sp^2. This seems to agree with the found transition state (Figs. 3a,b, and c), where the triple bond character in C–N disappears. The values of C–N bond lengths (represented as C(18)–N and C(9)–N) and C–C–N angle (represented by C–C(18)–N and C–C(9)–N) can be compared in the Table 4.

Lasperas *et al.* (15a) proposed a mechanism for the hydration step on protonic zeolites, in which the nucleophilic attack by water on protonated acetonitrile is coupled with a proton transfer to another water molecule. However, Sugiyama *et al.* (5), using manganese dioxide to hydrolyze acrylonitrile, suggested that proton transfer, which restores the active sites (OH groups on the surface), occurs by back donation from the nucleophile agent. Both ideas are analogous to our reaction path, in which all transition states

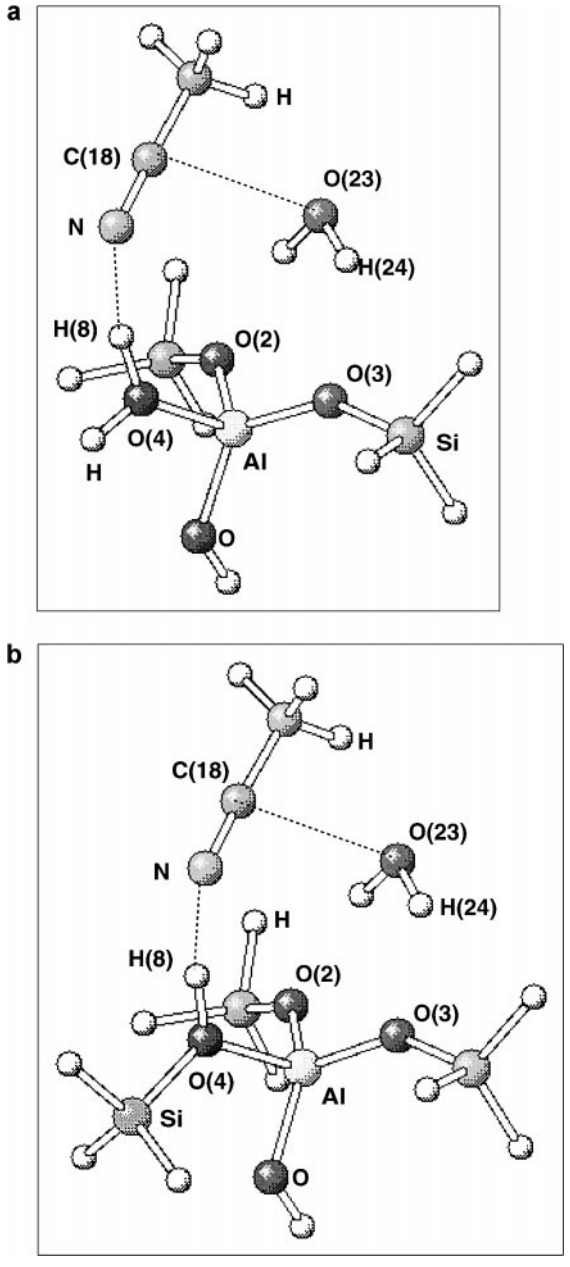

FIG. 2. (a) Acetonitrile, water molecule, and 3T model (3-dimensional configuration). (b) Acetonitrile, water molecule, and 4T model.

show that a water molecule is a nucleophile agent and source of protons simultaneously. Moreover, all transition states found also describe a concerted mechanism for the hydration.

In the $HCl(H_2O)_2$ cluster system, the second water molecule stabilizes the transition state, as previously verified by the authors elsewhere (47a). Hydrogen H(5) is donated to Cl, which a is stronger Lewis base than a water molecule. Applying the same analysis to the zeolite cluster, one can see that hydrogen is not back-donated to the same oxygen site. Instead, it goes to another one, which is also a strong Lewis base. Although the proton donation follows a different path, both systems behave similarly. The nonsolvated HCl has a reactivity similar to that of the protonic zeolite.

The ancillary effect of water molecules has also been studied by adding an extra water molecule into the zeolite model. In this case, the extra water molecule acts as a bridge for the back donation (see Fig. 3d—Ts1-4T-1w).

However, it is important to note that a simple difference between the activation energies of these two systems, with and without the extra water molecule, can lead to misinterpretation. This misinterpretation occurs due to the stabilization energy of reactants, which was not taken into account in this calculation (47a). Therefore, it becomes necessary to calculate only the stabilization energy ($\Delta E_{st}(Ts)$) and the stabilization free energy ($\Delta G_{st}(Ts)$) of the transition state, which is described by

$$\Delta E_{st}(Ts) = E(Ts1//(n+1)w) - (E(Ts1//(n)w) + E(\text{water})). \quad [1]$$

$E(Ts1//(n+1)w)$ is the calculated energy of the transition state configuration with $(n+1)$ water molecules and $E(\text{water})$ is the calculated energy of one isolated water molecule. This energy difference is shown in the Table 3. $\Delta E_{st}(Ts) < 0$ means the hydration transition state is stabilized by this extra water molecule. Interestingly, the stabilization effect found here, about 30 kJ/mol for the DFT method is not pronounced compared to previous work (47a), in which this stabilization was 60 kJ/mol for the DFT method.

This process is not favorable (its $\Delta G_{st}(Ts) > 0$) since the addition of an extra water molecule creates a steric hindrance for acetonitrile, which can be seen by comparing the dihedral angle between the atoms N, O(4), Al, and O(23) in the Ts1 and Ts1-(3/4T)-1*w* (see Table 4). The higher deviation from the coplanarity, the lower the stabilization energy. The active species are not in the best position to overlap their orbitals.

None of these results predicts the stepwise mechanism commonly verified in aqueous acid solution (3), which corresponds to a fast protonation followed by the nucleophilic attack. Only calculations with the $H_3O^+(H_2O)_2$ cluster show that acetonitrile is directly protonated (47a).

However, this activation energy is higher than that for the stepwise mechanism (see Table 3). Since the stepwise activation energy is only water nucleophilic attack energy, the proton donation energy is the main factor for the high barrier found for the concerted mechanism. Subtracting the activation barrier energy found for the $H_3O^+(H_2O)_2$ model from the one for zeolite and for the $HCl(H_2O)_2$ model, this proton donation energy for the concerted process can be calculated. This energy has the same magnitude for both Brønsted acid catalysts (zeolite or $HCl(H_2O)_2$ models) and

TABLE 3

Energies for Hydration Step (DFT/B3LYP), in kJ/mol

Step	Models				
	$HCl(H_2O)_2$	$H_3O^+(H_2O)$ (47a)	Zeolite 3T model	Zeolite 4T model	Zeolite 5T model
Hydration					
Heat of reaction					
MP2	45.9, 37.6[a]		39.8	22.8	
DFT	7.0, 6.3[a]		22.5	3.5	
Activation energy					
MP2	116.7	25.1	111.2	104.3	
DFT	78.2	3.2	75.9	70.9	
Ancillary effect of water					
ΔE_{st}(Ts)–DFT			−32.5	−26.5	
ΔG_{st}(Ts)–DFT			2.5	8.6	

Calculated energies for isomerization step (DFT/B3LYP), in kJ/mol

	$HCl(H_2O)_2$	$H_3O^+(H_2O)$ (46a)	Zeolite 3T model	Zeolite 4T model	Zeolite 5T model
Isomerization					
Activation energy					
2 : *syn*-isomer					
MP2	22.7				
DFT	13.5				
syn : *anti*-isomer					
RHF	91.5			95.5	
MP2	—			102.7	
DFT	—			84.9	
Uncatalyzed (DFT)				82.6	
anti-isom : acetamide					
RHF	−0.50			157.4	
MP2	—			126.8	
DFT	—			109.2	
Uncatalyzed (DFT)				120.1	
syn-isom : acetamide					
MP2	−67.3			4.72[b]	
DFT	88.4			−3.80[b]	10.5

[a] This reaction forms the protonated form of acetamide.
[b] Reaction heat corresponded to *syn*-isomer.

is approximately 90 and 70 kJ/mol for MP2/RHF and DFT methods, respectively.

In the case of Zn-exchanged zeolite (48), acetonitrile is activated by zinc ion (Lewis acid) and not by proton transfer. For the preferred reaction path, the activation energy for hydration (nucleophilic attack) is 25.8 kJ/mol. In a different path using the same catalyst, the value of the activation energy increases to 66.2 kJ/mol, since acetonitrile is protonated. One can conclude that the key of the hydration step is the activation of the reactants, mainly acetonitrile.

Analyzing the activation energy values, both zeolite and $HCl(H_2O)_2$ models predict a lower energy than the experimental value, 127.3 kJ/mol (14d). DFT, in some cases, underestimates calculated energies (24, 29, 49) and activation energies (50). MP2 values, in most of the cases found here, have a larger difference in comparison to DFT. This difference can be caused by two different factors. For the zeolite model MP2 energies are calculated from the geometries obtained at the RHF level (single-point calculations), and for both models the basis set used in our calculations is not large enough to describe correctly the MP2 energy of hydrogen-bonding complexes, as has been recently shown in (51).

3.2.2. Isomerization of the Intermediate

The first product of the hydration of acetonitrile is not acetamide (Ac), but an intermediate molecule (hydroxy

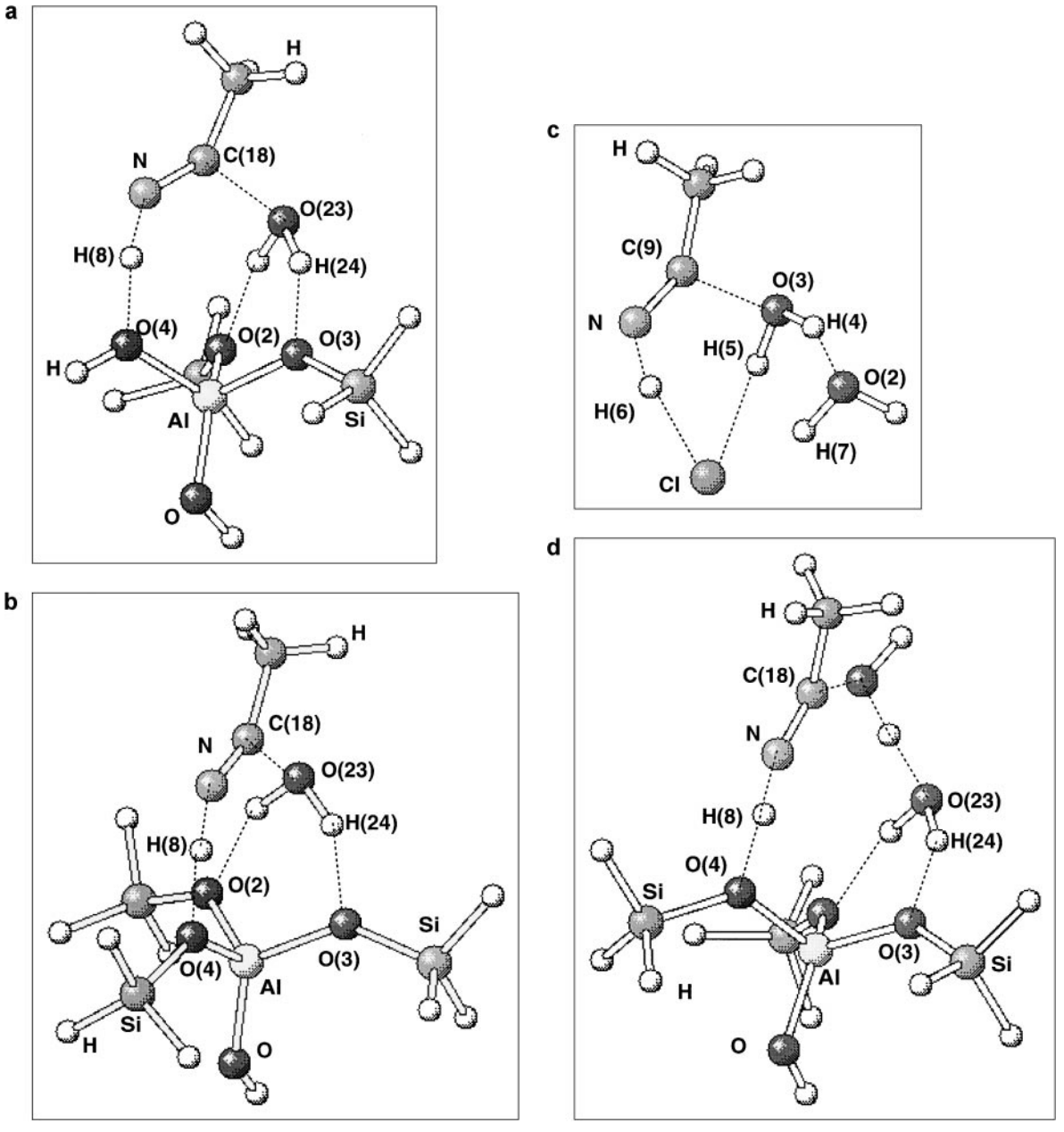

FIG. 3. (a) Transition states of the hydration reaction found using 3T model (3-dimensional configuration)—Ts1-3T. (b) Transition states of the hydration reaction found using 4T model—Ts1-4T. (c) Transition states of the hydration reaction found using $HCl(H_2O)$ model—Ts1. (d) Transition states of the hydration reaction found using 4T model with one extra water molecule—Ts1-4T-1*w*.

imine) that changes into acetamide. This intermediate has been identified in a number of previous studies, such as on unactivated alumina (6), on Pd(II) (7) and dirhenium (8) complexes, on zinc-substituted zeolites (48), hydrochloric acid (47a), and protonic zeolites (23). This intermediate molecule has four different isomers (Fig. 4a). Each of them differs simply from others by rotation of an OH or NH group. The latter transformation is the most difficult, since it is a rotation of a double bond. The equilibrium constants for the isomerization in gas phase among all configurations were calculated using the following expression:

$$_{298}K^{o} = \exp(-\Delta_{298}G^{o}/(RT)). \qquad [2]$$

All these values are available when the zero-point energy is computed by Gaussian 94 code (32).

The equilibrium constant values suggest that the configuration 4 (*anti*-isomer) is more stable than the other iminol isomers in the gas phase (see Table 5). This *anti*-isomer is also the most stable form among the isomers of formamidic

TABLE 4

Optimized Geometries for the Hydration Transition State (DFT/B3LYP)

	Zeolite model			$HCl(H_2O)_2$ model		
	Ts1-3T	Ts1-4T	Ts1-3T-1*w*	Ts1-4T-1*w*	Ts1	Experiment[a]
N–H(8)	1.11	1.11	1.13	1.11		—
N–H(6)					1.10	
C(18)–N	1.20	1.20	1.20	1.20		1.27
C(9)–N					1.20	
O(3)–H(24)	1.66	1.69	1.72	1.73		—
O(2)–H(25)	1.66	1.69	1.74	1.77		—
Cl–H(5)					2.18	—
C(18)–O(23)	1.82	1.88	1.76	1.79		1.36
C(9)–O(3)					1.92	
N–C(18)–O(23)	118.9°	117.8°	118.6°	117.6°		—
N–C(9)–O(3)					113.8°	
C–C(18)–N	141.5°	143.7°	139.1°	140.2°	—	—
C–C(9)–N						
N–O(4)–Al–O(23)	0.99°	0.00°	−17.9°	−24.3°	—	—

Note. All distances are in angstroms (Å) and angles in degrees.
[a] Refers to experimental values in Å (48); C–OH, from acetic acid; C=N, from methyleneimine.

acid. However, formamide is more stable than this isomer by 47.0 kJ/mol at MP4//MP2/6-311++G(2d, 2P) (52). Both results are in complete agreement with our results (see again Table 5). Our equilibrium constant for tautomerism is also in good agreement with other examples, such as the equilibrium constant found for the tautomerism of 9-acridamine into 9(10*H*)-acridinimine (53). The value found was 0.787 (RHF) and 0.107 (DFT) at 298 K.

TABLE 5

Relation between Intermediate Isomers and Acetamide, Energies in kJ/mol

Configuration	Relative energy to *syn*-isomer		Equilibrium constants ($_{298}K^{\circ}$)	
	DFT	MP2	DFT	MP2
syn	0.0	0.0	*syn* → 2 0.284	*syn* → 2 0.176
2	+3.2	+4.4	2 → 3 $4.32\ 10^{-3}$	2 → 3 $3.19\ 10^{-3}$
3	+17.0	+19.0	*anti* → 3 $5.34\ 10^{-6}$	*anti* → 3 $2.17\ 10^{-6}$
anti	−13.3	−11.9	Ac → *anti* $1.65\ 10^{-12}$	Ac → *anti* $1.69\ 10^{-11}$
	Relative energy to *syn*-isomer		Proton affinity NH_2	 C=O
Acetamide (Ac)	−76.5	−71.9	RHF −803.8 DFT −812.7 MP2 −821.8	RHF −884.5 DFT −869.3 MP2 −864.2
			Proton affinity	
NH_3			DFT −865.4	MP2 −866.2

For the $HCl(H_2O)$ model configuration 2 is the product of acetonitrile hydration (see Scheme 3). This is not a stable configuration, therefore it isomerizes into acetamide in several steps. Initially, this isomer changes into an *syn*-isomer by simple C–OH bond rotation, which requires low activation energy, 13.0 kJ/mol (see Table 3). The next step is to transform *syn*- into *anti*-isomer by C=NH bond rotation. At last, *anti*-isomer tautomerizes into acetamide.

Using the RHF method all steps could be calculated (see Scheme 3a). The isomerization-limiting step is the formation of *syn*-isomer, which needs high activation energy, 118.9 kJ/mol. In the case of the tautomerization step, it happens without activation energy (a negative value was found after ZPE correction—see Table 3). A similar result is obtained using DFT and MP2 methods, but the tautomerism occurs directly from *syn*-isomer (see Scheme 3b). All attempts to optimize the *anti*-isomer configuration using the latter two methods resulted in the acetamide configuration. This result was expected, because the equilibrium constant between these two isomers is far more favorable to amide (see Table 5). Previously the authors have found the same result studying different proton donor catalysts for the tautomerism reaction (47a). Finally, the isomerization on $HCl(H_2O)$ model occurs in two steps: the rotation of C–OH bond and tautomerization, which happens simultaneously with the C–NH rotation.

The 3T zeolite model demonstrates deficiency in predicting the isomerization transition states, because of the problems mentioned previously. Instead, the 4T model describes the isomerization by two different reaction paths (see Scheme 4). The first idea is very similar to the "homogeneous model" reaction path (see Scheme 4a). However,

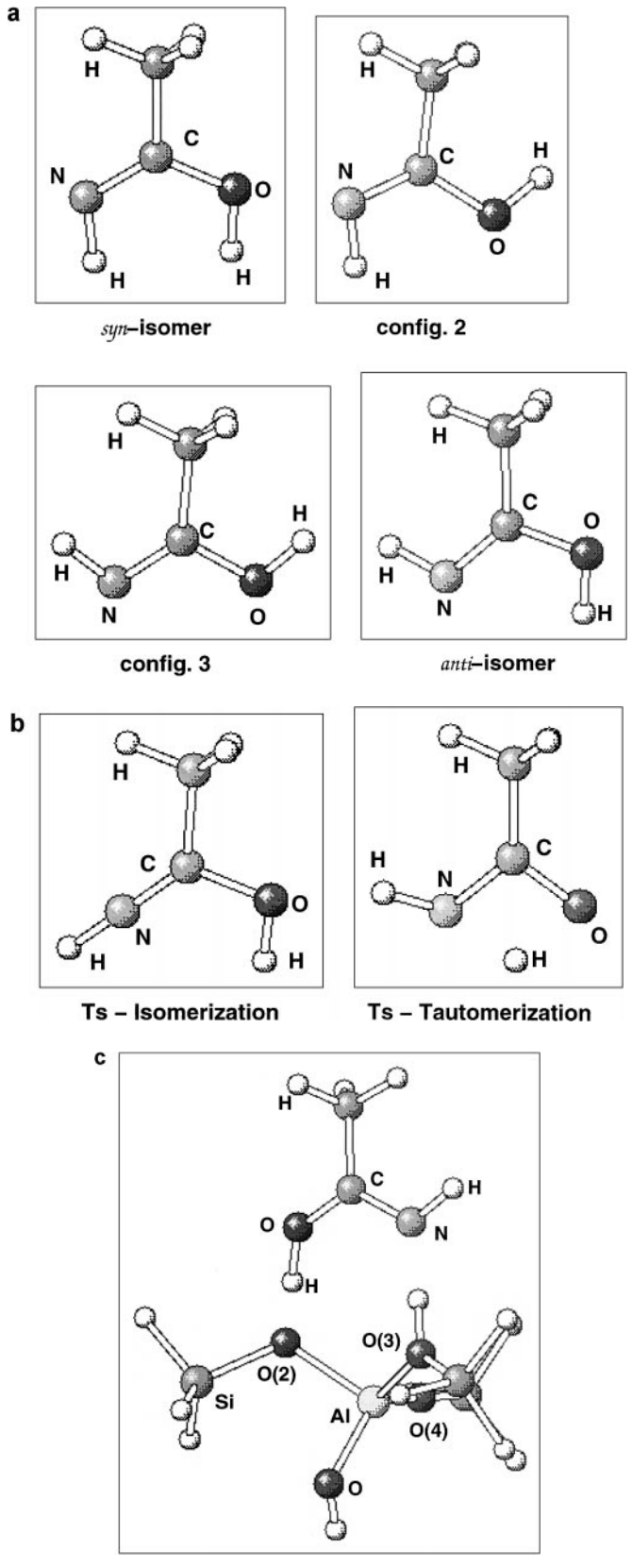

FIG. 4. (a) Different isomers of the intermediate. (b) Isomerization and tautomerization transition states. (c) *Anti*- isomer and 4T model (this is not an optimized geometry).

there are few differences, and the main one is that the hydration product is not configuration 2, but a *syn*-isomer. Therefore, this path has only two steps: formation of *anti*-isomer and tautomerism. Both transition states require high activation energy, 84.9 and 109.2 kJ/mol for isomerism and tautomerization, respectively (for the DFT method, see Table 3). Surprisingly, the tautomerism barrier is even higher than the hydration activation energy (see Scheme 4a).

Another interesting point is that these two processes are very similar to the uncatalyzed ones (see Fig. 4b). The transition states have similar optimized geometry, as well as the activation energies, 82.6 and 120.1 kJ/mol for isomerism and tautomerization, respectively (see Table 3). The zeolite model does not influence the mechanism, since neither NH nor OH groups have been activated by the catalyst model in the transition state.

However, the tautomerism can be assisted by water molecules. This proton transfer assistance has been observed for other different molecules, such as *N*-nitrobenzenesulfonamides (54), isocyanates (19), β-lactams (20), and carbodiimine (21). An acillary effect was also studied by the authors previously in the same reaction on different catalysts (47a, 48). This synergetic effect can reduce the activation energy up to 100 kJ/mol, favoring the tautomerism.

The *anti*-isomer could also adsorb in a different manner. The NH group instead of the OH group interacts with the Brønsted site (see Fig. 4c). In this case, all our attempts resulted in the acetamide configuration, similar to the "homogeneous model" result. The NH group seems to be very reactive, accepting the proton easily. In all these cases, acetamide is the final configuration.

The second idea is to start again from *syn*-isomer. In this case, this molecule desorbs from the Brønsted site to readsorb in a different configuration, so-called N configuration (see Scheme 4b). The new configuration differs from the initial one by the H-bonding group: NH (N configuration) instead of OH. As mentioned before, the NH group is very reactive; thus its protonation occurs with very low barrier energy, or even no barrier (the DFT calculation corrected with ZPE gives a negative value). This configuration is the protonated acetamide. The intermediate is the first step for the amide hydrolysis as described in previous studies (54, 55), which means that hydrolysis may result directly in carboxy acid. However, protonated intermediate configuration is not stable in this model. Even after fixing the NH group in the N–H(9)–O(3)–O(2) and the N–H(8)–O(2)–O(3) planes, this configuration was not obtained, regardless of the method used. There are two different effects occurring simultaneously. The first is that the 4T model geometry is distorted when the proton is donated (see Fig. 5a). The SiH_3 group moves up and creates a repulsive interaction with the protonated molecule. This destabilizes the system, shifting the configuration back to the neutral molecule (later another example of this effect

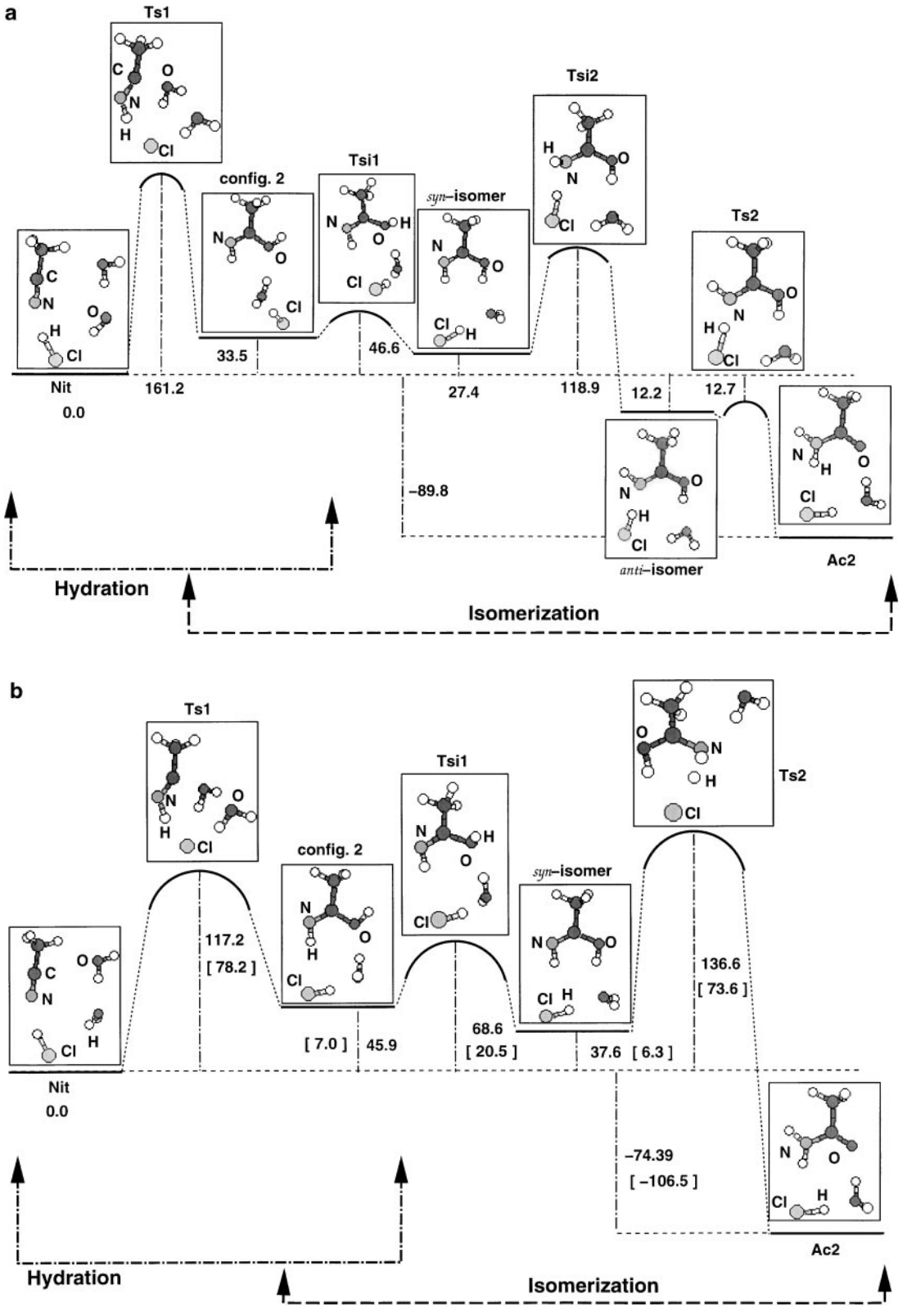

SCHEME 3. (a) RHF energy diagrams—hydrolysis on $HCl(H_2O)_x$ cluster models. (b) DFT and MP2 energy diagram—hydrolysis on $HCl(H_2O)_x$ cluster models.

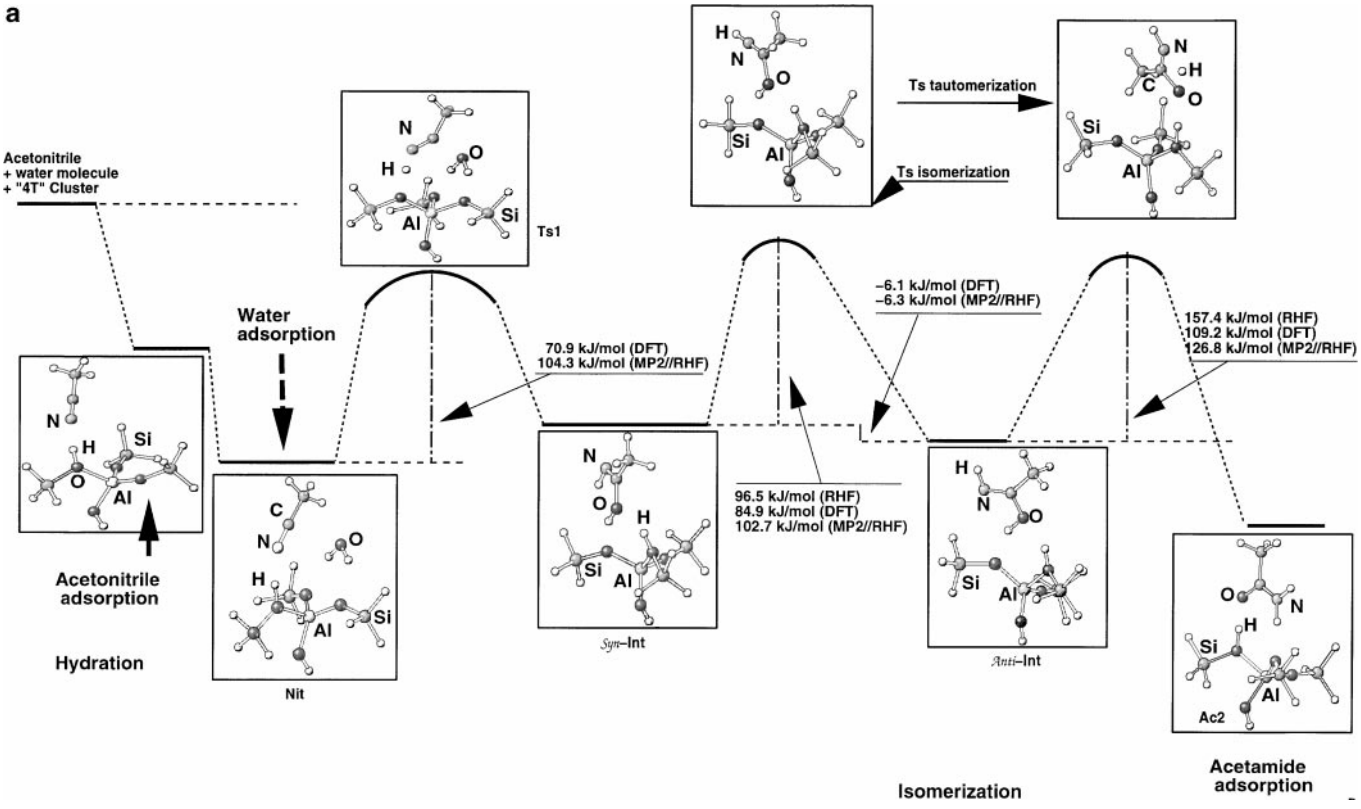

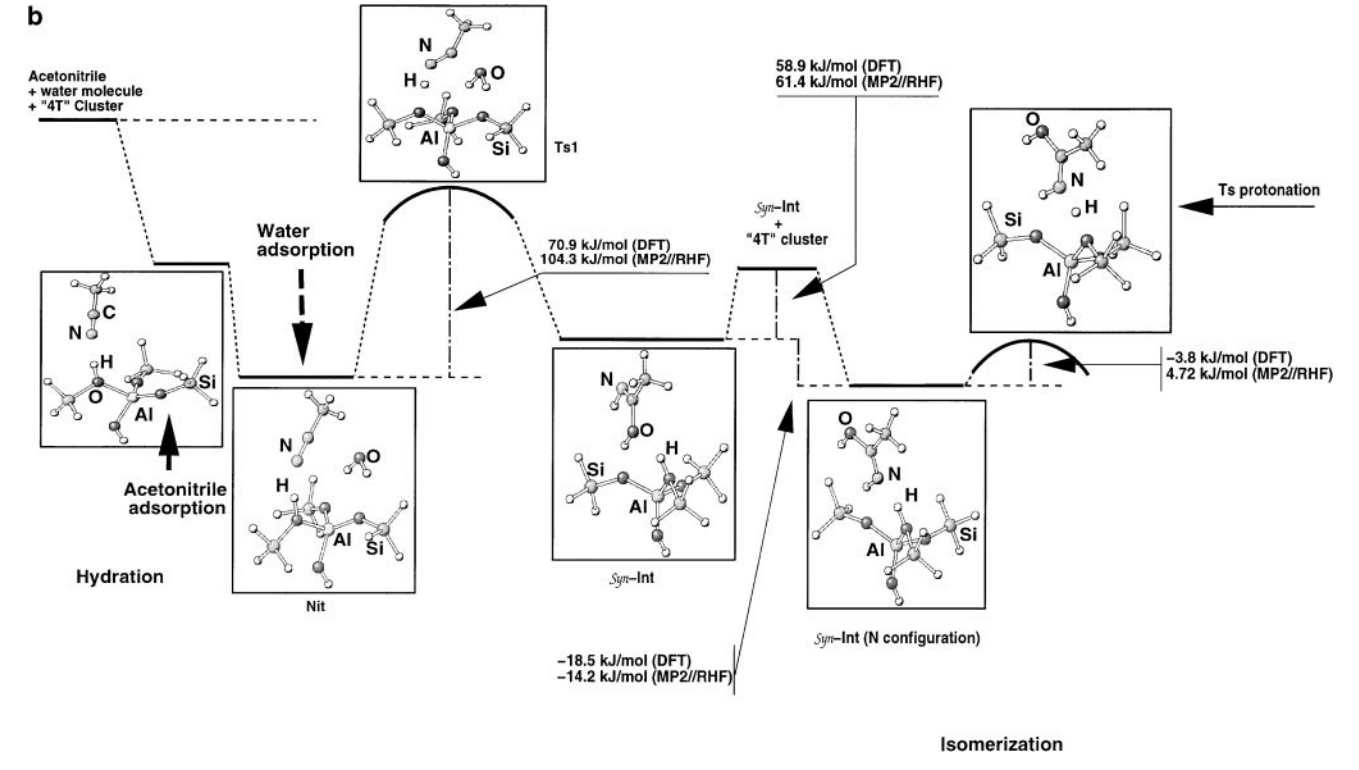

SCHEME 4. (a) DFT and MP2//RHF energy diagram—hydrolysis on 4T model. (b) DFT and MP2//RHF energy diagram—hydrolysis on 4T model. (c) DFT energy diagram—5T model.

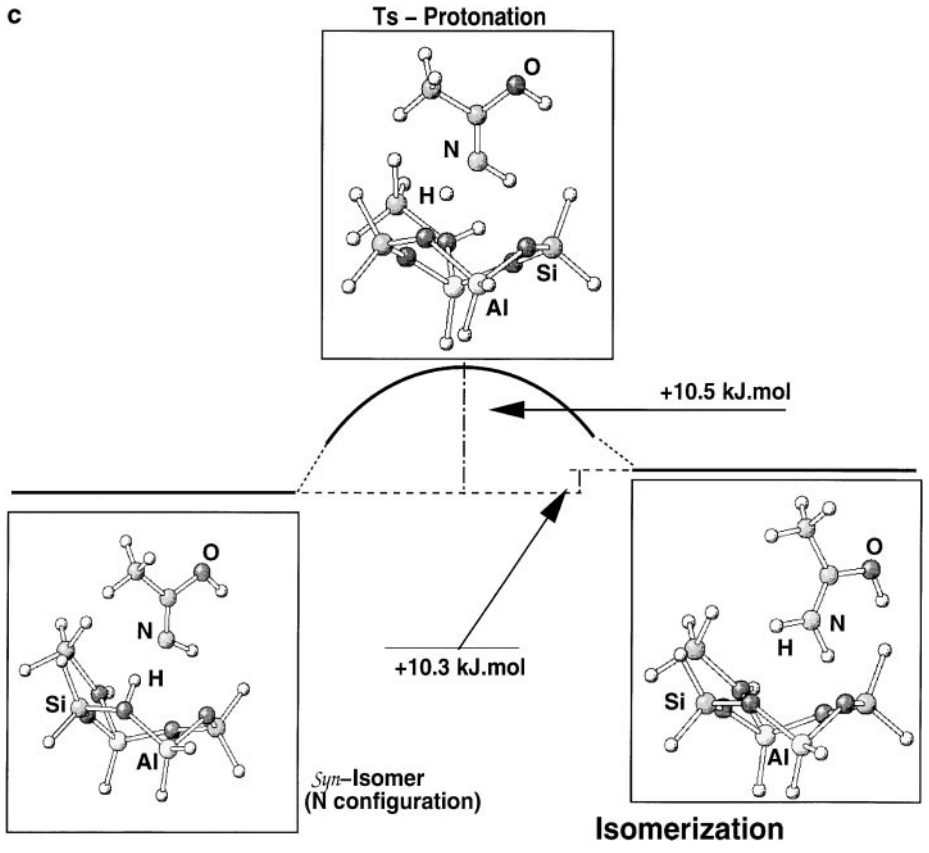

SCHEME 4—*Continued*

will be shown). The second effect explains the instability of the protonated molecule. The cluster approach does not take in account the stabilization effects produced by van der Waals interaction of the positive charged molecule with the zeolite cavity oxygen atoms.

The model size was increased to a 5T configuration (Si/Al = 1.5), which is composed by one 4T ring plus an $OSiH_3$ branch. Even though this model has one more Brønsted site than the 3T and 4T models, the acidity of all these zeolite models is quite similar, see Table 2. Our aim was to study the protonation of the group NH, avoiding the geometric distortions that occurred with the use of the 4T model. In this case, only DFT calculations were done, see Scheme 4c. A similar result was obtained, except that the activation barrier was not negligible as before: 10 kJ/mol (see Table 3). The protonated intermediate is also not stable; however, the previous constraints used for the 4T model resulted in a final optimized geometry, which had no negative frequencies. Although this approach avoids the geometric distortions, the model is still far from the real zeolite system.

3.2.3. Amide Desorption

Despite the fact that the most favorable isomerization path does not form acetamide directly but possibly its O-protonated form, three different configurations for acetamide adsorption were studied. These configurations differ by changing the H bond between acetamide and zeolite model (see Fig. 5b). The first structure is called configuration Ac2, in which both CO and NH_2 groups interact with the cluster model. However, the main H bond is between CO and the Brønsted site. The second configuration (Ac1) has only an NH_2 group interacting with the Brønsted site. The last configuration (Ac3) is the N-protonated form of acetamide.

Ac2 is the most stable acetamide configuration. The energy difference between Ac2 and Ac1 is about 40 kJ/mol (see Table 2), regardless of the method and cluster model used. This configuration stabilization is in line with the idea that the higher number of hydrogen bonds formed, the more stable the adsorbed species (56).

Ac2 requires higher desorption energy compared to acetonitrile, thus indicating that it is a potential inhibitor for acetonitrile hydrolysis. This poisoning effect has been previously observed in experimental studies, such as in ethyl ester synthesis from aromatic nitriles on acid zeolites (15a) and in the liquid phase hydration of acrylonitrile on manganese dioxide catalyst (5).

The desorption of Ac2 can be promoted by the reactants, restoring the catalytic cycle (Scheme 5). Both reactants decrease the energy needed for Ac2 desorption by 50 kJ/mol. However, the process is still endothermic.

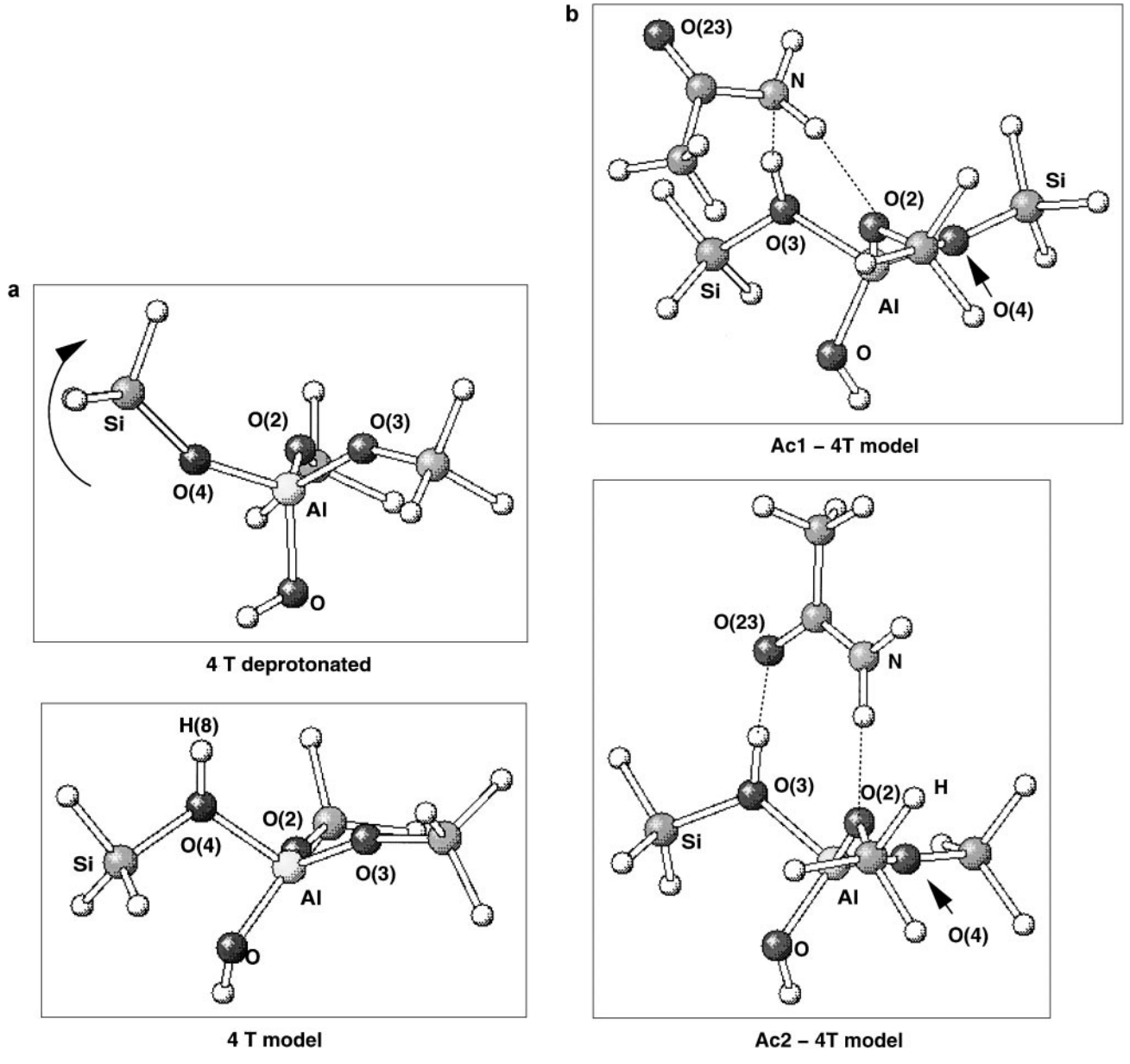

FIG. 5. (a) 4T model problems. (b) Different configurations of acetamide adsorption on 4T model (Ac1 and Ac2). (c) Ac3 configuration of acetamide on different cluster models (3T model and 4T model. (d) Different configuration of acetamide on $HCl(H_2O)$ model.

This promoted desorption is better illustrated by using a Zn-exchanged zeolite to catalyze the nitrile hydrolysis (48). Water and acetonitrile can displace acetamide from the active site (Zn^{2+}) in a exothermic process.

For Ac1 configuration (Fig. 5b), nitrogen from the NH_2 group interacts with the zeolite proton. At the same time, one of the zeolite oxygen atoms forms another H bond with the same NH_2 group. Although this configuration has two H bonds, both bonds are weaker than those for the Ac2 configuration (compare the distances O(24)–O(3) and N–O(2) in Ac2 to N–O(3) and N–O(2) in Ac1, Table 1).

This bidentate configuration is very similar to the ammonia bidentate configuration (55); however, in the latter case nitrogen is protonated by the zeolite cluster. Interestingly, the methyl group of acetamide moves away from O(4)H (3T model) and $OSiH_3$ (4T model) groups, see Fig. 5b for the 4T model, to avoid a repulsive interaction between these cluster groups and acetamide molecule.

Ac3 (the protonated Ac1 form) forms three hydrogen bonds with the cluster (Fig. 5c). The protonation energy (difference between Ac3 and Ac1 adsorption energies) has positive values, 57.3, 29.7, and 30.3 kJ/mol for RHF, MP2//RHF, and DFT methods, respectively (using either the 3T or the 4T model), which indicates an endothermic process. Moreover, the Ac1-binding energy (see Table 2) has a very low value (about 10 times less) compared to

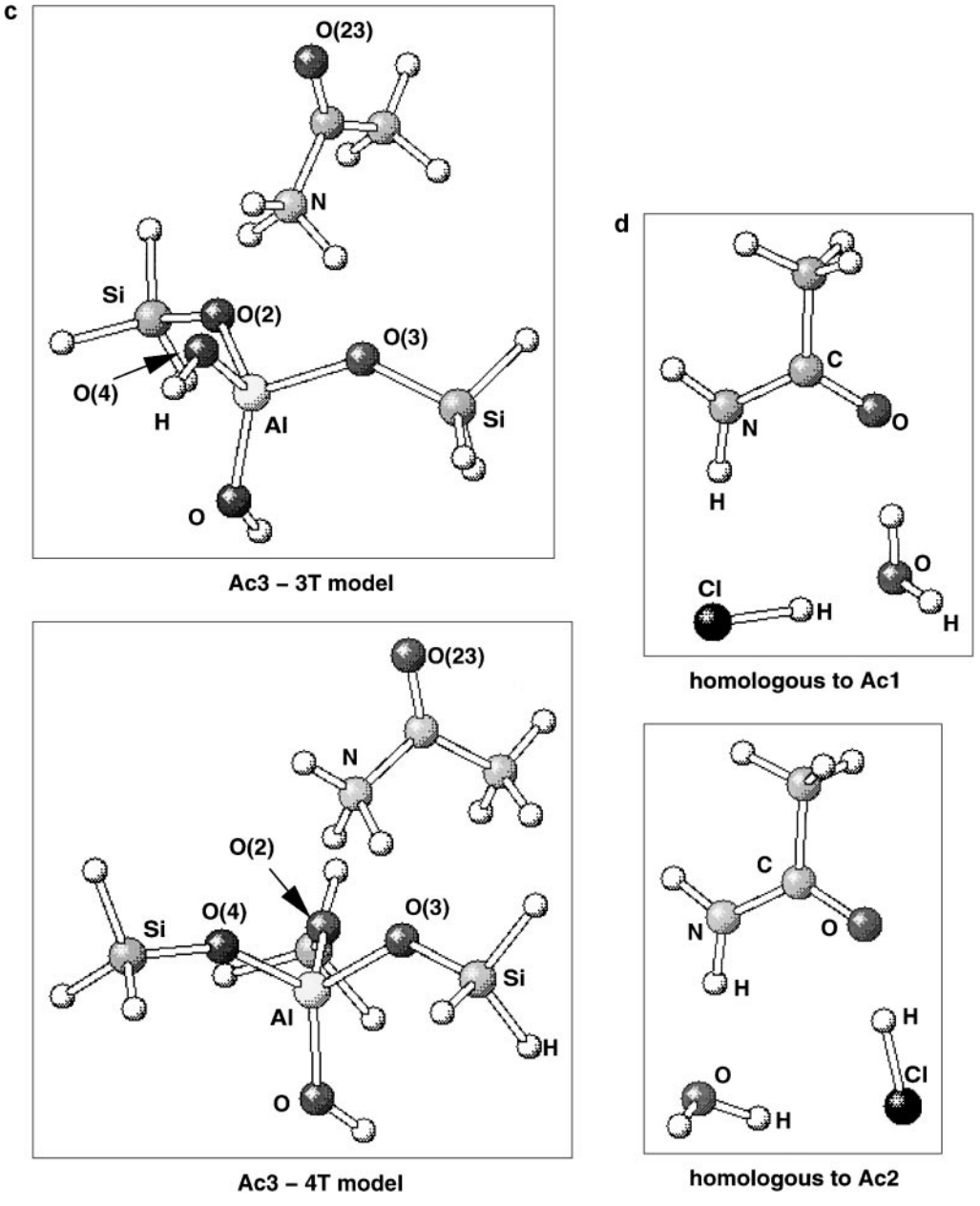

FIG. 5—*Continued*

that previously calculated for different organic amines and ammonia, which ranges from 145 kJ/mol for ammonia to 230 kJ/mol for 2-methylpyridine (18b). Both results indicate that the NH_2 group from acetamide is not a good proton acceptor.

Two remarks are necessary about the latter results. First, the RHF method shows results quite different from those of DFT and MP2//RHF, thus indicating that electron correlation is recommended for calculating for charged species. Second, the 4T cluster model was partially constrained (the hydrogen atoms from all SiH_3 groups were frozen in their spatial position) for the DFT calculation. These constraints prevented the repulsive effect of the $OSiH_3$ group, which moves up (Si–O–Al angle becomes close to 180°) and pushes acetamide molecules away during the optimization process. Without those constraints, the final configuration obtained was the Ac1 configuration. However, this effect has not been observed for the 3T model, because the OH group has less volume than the $OSiH_3$ group. This effect is equal to that previously observed in our study of the isomerization mechanism.

To complement this study, the proton affinity of C=O and NH_2 of acetamide was compared, since there are two possibilities of acetamide protonation: N and O protonation.

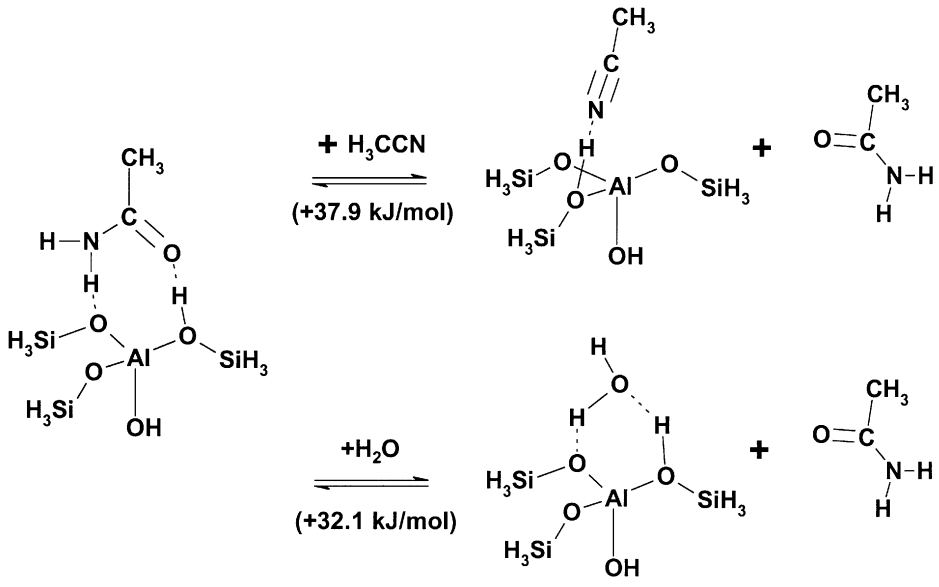

SCHEME 5. Desorption of acetamide promoted by the reactants.

This affinity is calculated by subtracting the neutral molecule energy from its protonated form energy:

$$P_{\text{affinity}} = E_{\text{neutral molecule}} - E_{\text{protonated molecule}}. \qquad [3]$$

The C=O group has higher proton affinity than the NH_2 group. This affinity is even comparable to the value of ammonia (see Table 5). Previously, different studies, such as of ketones adsorption (22 g) and aromatic amides hydrolysis (57) on zeolites, showed that the C=O group interacts directly with the cluster proton. Combining both results, one can conclude that acetamide will certainly be O-protonated on zeolites, which agrees with the current proposed mechanism of acid-catalyzed hydrolysis for regular amides (e.g., acetamide) (54).

For the $HCl(H_2O)$ model, the energy difference between the two possible acetamide configurations, which are homologous to Ac1 and Ac2 configurations (see Fig. 5d), is not large. This difference has the following values, 4.9 and 5.8 kJ/mol for MP2 and DFT, respectively. Therefore, acetamide has no preference for interacting with the different $HCl(H_2O)$ model configurations.

4. CONCLUSIONS

The hydrolysis of nitriles has been studied theoretically by different *ab initio* methods (RHF, DFT, and MP2). Two Brønsted acid models have been compared: zeolite and $HCl(H_2O)_{x=2.,1}$ clusters. Both catalysts are found to behave similarly. For example, acetonitrile prefers to adsorb without protonation on both models, demonstrating that the zeolite is not a super acid, since experimental studies have shown that acetonitrile can be protonated in a super-acid medium as FSO_3H–SBF_5–SO_2 solution (58).

The hydrolysis reaction can be divided in three well-defined steps: hydration, isomerization of the intermediates, and desorption of acetamide. The hydration mechanism is very sensitive to the acid strength. In strong acid, the protonation occurs without barrier, thus the mechanism of hydration follows a stepwise pathway. In the case of both Brønsted acids studied here, a concerted mechanism is preferred.

The isomerization pathway depends on the catalyst. For the "homogeneous model," this mechanism has more steps than for the zeolite model, such as rotation of C–OH bond, rotation of C–NH bond, and tautomerism. However, the zeolite catalyst leads to two different paths. One forms acetamide directly, the other forms its O-protonated configuration, which is the first step for acetamide hydrolysis. This path seems to be preferred, since low activation energy is required and it can lead directly to the carboxy acid formation.

Acetamide can be adsorbed in three different ways on zeolite cluster. The most stable configuration (Ac2) has higher desorption energy than acetonitrile and it may certainly poison the catalytic site. However, this desorption energy can be reduced by displacing acetamide with either water or acetonitrile, which restores the catalytic cycle.

For the zeolite catalyst the overall rate-limiting step is the hydration since the isomerization step is assisted by water molecules and the displacement of acetamide from the catalytic site is promoted by the reactants. On the other hand, the overall rate-limiting step in the homogeneous case is either the hydration or the isomerization step.

The van der Waals interactions play an important role in this reaction. Due to these interactions, oxygen atoms of the zeolite cavity can stabilize charged species as N- and O-protonated acetamide configurations.

ACKNOWLEDGMENTS

L. A. M. M. Barbosa thanks the National Council of Scientific and Technologic Development (CNPq, Brazil) for the scholarship and Dr. Fréderic Fréchard for useful discussions. This work has been performed under auspices of NIOK, the Netherlands Institute for Catalysis Research, Lab Report No. TUE-99-5-10.

REFERENCES

1. (a) Clerici, M., G., *Appl Catal.* **68**, 249 (1991); (b) Cavani, F., Centi, G., and Trifiró, F., *Chim. Ind.* **74**, 182 (1992); (c) Chen, J. D., Daka, J., Neelma, E., and Seldom, R. A., *J. Chem. Soc. Chem. Commun.*, 1379 (1993); (d) Riguto, M. S., and van Bekkun, H., *J. Mol. Catal.* **81**, 77 (1993); (e) Tuel, A., and Ben-Taarit, Y., *Appl. Catal. A* **102**, 201 (1993).
2. "Ullman's Encyclopedia of Industrial Chemistry" (Weinheim, Ed.), Vol. A26, p. 198, 1985–1996.
3. Schaefer, F. C., *in* "The chemistry of Cyano Group" (Z. Rappoport, Ed.), Chap. 6. Interscience, New York, 1970.
4. Izzo, B., Harrell, C. L., and Klein, M. T., *AIChE J.* **43**, 2048 (1997).
5. Sugiyama, K., Miura, H., Nakano, Y., Suzuki, H., and Matsuda, T., *Bull. Chem. Soc. Jpn.* **60**, 453 (1987).
6. Wilgus, C. P., Downing, S., Molitor, E., Bains, S., Pagni, R. M., and Kaballa, G. W., *Tetrahedron Lett.* **36**, 3469 (1995).
7. Kaminskaia, N. V., and Kostié, N. M., *J. Chem. Soc. Dalton Trans.*, 3677 (1996).
8. Bauer, C. B., Concolino, T. E., Eglin, J. L., R. D., and Staples, R. J., *J. Chem. Soc. Dalton Trans.*, 2813 (1998).
9. Aboulayt, A., Binet, C., and Lavalley, J.-C., *J. Chem. Soc. Faraday Trans.* **91**, 2913 (1995).
10. Sugiyama, K., Miura, H., Watanabe, Y., Ukai, Y., and Matsuda, T., *Bull. Chem. Soc. Jpn.* **60**, 1579 (1987).
11. Prihod'ko, R., Kolomitsyn, I., Sychev, M., Stobbelaar, P. J., and van Santen, R. A., submitted for publication.
12. Izumi, Y., *Catal. Today* **33**, 371 (1997).
13. (a) Cohen, M. A., Sawden, J., and Turner, N., *Tetrahedron Lett.* **49**, 7223 (1990); (b) Cohen, M. A., Parrat, J. S., and Turner, N., *Tetrahedron: Asymmetry* **3**, 1543 (1992); (c) Ashima, Y., and Suto, M., *in* "Industrial Applications of Immobilized Bio-catalysts" (A. Tanaka, T. Tosa, and T. Kobayashi, Eds.), p. 91. Marcel Dekker, New York, 1992; (d) Berad, T., Cohen, M. A., Parrat, J. S., and Turner, N., *Tetrahedron: Asymmetry* **4**, 1085 (1993); (e) Crosby, J., Moilliet, J., Parrat, J. S., and Turner, N., *J. Chem. Soc. Perkin Trans.* **1**, 1679 (1994); (f) Meth-Cohn, O., and Wang, M.-X., *J. Chem. Soc. Perkin Trans.* **1**, 1099 (1997); (h) Matoishi, K., Sano, A., Imai, N., Yamazaki, T., Yokoyama, M., Sugai, T., and Otha, H., *Tetrahedron: Asymmetry* **9**, 1097 (1998); (i) Bauer, R., Knackmuss, H.-J., and Stolz, A., *Appl. Microbiol. Biotechnol.* **49**, 89 (1998).
14. (a) Krieble, V. K., and McNally, J. G., *J. Am. Chem. Soc.* **51**, 3369 (1929); (b) Krieble, V. K., and Noll, C. I., *J. Am. Chem. Soc.* **61**, 561 (1939); (c) Rabinovitch, B. S., Winkler, C. A., and Stewart, A. R. P., *Can. J. Res.* **20**, 121 (1942); (d) Belsky, A. J., and Brill, B. T., *J. Phys. Chem. A* **103**, 3006 (1999).
15. (a) Lasperas, M., Graffin, P., and Geneste, P., *J. Catal.* **139**, 362 (1993); (b) Vital, J., and Valente, H., *in* "Heterogeneous Catalysis and Fine Chemicals IV" (H. U. Blaser, A. Baiker, and R. Prins, Eds.), p. 555. Elsevier Science, Amsterdam, 1997; (c) Stepanov, A. G., and Luzgin, M. V., *Chem. Eur. J.* **3**, 47 (1997).
16. (a) Blaszkowski, S. R., Nascimento, M. A. C., and van Santen, R. A., *J. Phys. Chem.* **100**, 3463 (1996); (b) Boronat, M., Viruela, P. M., and Corma, A., *J. Phys. Chem. B* **101**, 10069 (1997); (c) Boronat, M., Viruela, P. M., and Corma, A., *J. Phys. Chem. A* **102**, 982 (1998).
17. (a) Blaszkowski, S. R., and van Santen, R. A., *J. Am. Chem. Soc.* **118**, 5152 (1996); (b) Sinclair, P. E., and Catlow, C. R. A., *J. Chem. Soc. Faraday Trans.* **93**, 333 (1997); (c) Sinclair, P. E., and Catlow, C. R. A., *J. Phys. Chem. B* **101**, 93 (1997).
18. (a) Pelmenschikov, A. G., van Santen, R. A., Janchen, J., and Meijer, E., *J. Phys. Chem.* **97**, 11071 (1993); (b) Gorte, R. J., and White, D., *Topics Catal.* **4**, 57 (1997); (c) Bell, A. T., *Catal. Today* **38**, 151 (1997); (d) Haw, J. F., Xu, T., Nicholas, J. B., and Goguer, P. W., *Nature* **389**, 833 (1997); (e) Meijer, E. L., van Santen, R. A., and Jansen, A. P., *J. Phys. Chem. B.* **103**, 2553 (1999).
19. Raspoet, G., Nguyen, M. T., McGarraghy, M., and Hegarty, A. F., *J. Org. Chem.* **63**, 6867 (1998).
20. (a) Wolfe, S., Kim, C. K., and Yang, K., *Can. J. Chem.* **72**, 1033 (1994); (b) Pitarch, J., Ruiz-López, M. F., Silla, E., Pauscual-Ahuir, J.-L., and Tuñón, I., *J. Am. Chem. Soc.* **120**, 2146 (1998).
21. Lewis, M., and Glaser, R., *J. Am. Chem. Soc.* **120**, 8541 (1998).
22. (a) Kazansky, V. B., *Acc. Chem. Res.* **24**, 379 (1991); (b) Sierra, L. R., Kassab, E., and Evleth, E. M., *J. Phys. Chem.* **97**, 641 (1993); (c) Viruela-Martin, P., Zicovich-Wilson, C. M., and Corma, A., *J. Phys. Chem.* **97**, 13713 (1993); (d) Florian, J., and Kubelkova, L., *J. Phys. Chem.* **98**, 8734 (1994); (e) Kazansky, V. B., Frash, M., and van Santen, R. A., *Catal. Lett.* **28**, 211 (1994); (f) Kazansky, V. B., Senchenya, I. N., Frash, M., and van Santen, R. A., *Catal. Lett.* **27**, 345 (1994); (g) Xu, T., Munson, E. J., and Haw, J. F., *J. Am. Chem. Soc.* **116**, 1962 (1994); (h) Zicovich-Wilson, C. M., Viruela-Martin, P., and Corma, A., *J. Phys. Chem.* **99**, 13224 (1995); (i) Wilberg, K. B., Ochterski, J., and Streitwieser, A., *J. Am. Chem. Soc.* **118**, 8291 (1996).
23. Haw, J. F., Hall, M. B., Alvarado-Swaisgood, A. E., Munson, E. J., Lin, Z., Beck, L. W., and Howard, T., *J. Am. Chem. Soc.* **116**, 7308 (1994).
24. Gale, J. D., *Topics Catal.* **3**, 169 (1996).
25. Sauer, J., Ugliengo, P., Garrone, E., and Saunders, V. R., *Chem. Rev.* **94**, 2095 (1994).
26. Shah, R., Gale, J. D., and Payne, M. C., *J. Phys. Chem. B* **101**, 4787 (1997).
27. Dunning, T. H., Jr., and Hay, P. J., *in* "Modern Theoretical Chemistry" (H. F. Schaefer III, Ed.), p. 1. Plenum, New York, 1976.
28. (a) Sauer, J., *in* "Cluster Models for Surface and Bulk Phenomena" (G. Pacchioni, P. S. Bagus, and F. Parmigiani, Eds.), p. 533. Plenum, New York, 1992; (b) Haase, F., and Sauer, J., *J. Phys. Chem.* **98**, 3083 (1994).
29. Scheiner, A. C., Baker, J., and Andzelm, J. W., *J. Comput. Chem.* **18**, 775 (1997).
30. Nicholas, J. B., *Topics Catal.* **4**, 157 (1997).
31. (a) Koch, W., and Hertwig, R. H., *Chem. Phys. Lett.* **286**, 345 (1997); (b) Curtiss, L. A., Raghavachari, K., Redfern, P. C., and Pople, J. A., *Chem. Phys. Lett.* **270**, 419 (1997).
32. Gaussian 94, Revision E.2, Frisch, M. J., Trucks, G. W., Schlegel, H. B., Gill, P. M. W., Johnson, B. G., Robb, M. A., Cheeseman, J. R., Keith, T., Petersson, G. A., Montgomery, J. A., Raghavachari, K., Al-Laham, M. A., Zakrzewski, V. G., Ortiz, J. V., Foresman, J. B., Cioslowski, J., Stefanov, B. B., Nanayakkara, A., Challacombe, M., Peng, C. Y., Ayala, P. Y., Chen, W., Wong, M. W., Andres, J. L., Replogle, E. S., Gomperts, R., Martin, R. L., Fox, D. J., Binkley, J. S., Defrees, D. J., Baker, J., Stewart, J. P., Head-Gordon, M., Gonzalez, C., and Pople, J. A., Gaussian, Pittsburgh PA, 1995.
33. Gaussian 92/DFT, Revision G.4, Frisch, M. J., Trucks, G. W., Schlegel, H. B., Gill, P. M. W, Johnson, B. G., Wong, M. W., Foresman, J. B., Robb, M. A., Head-Gordon, M., Replogle, E. S., Gomperts, R., Andres, J. L., Raghavachari, K., Binkley, J. S., Gonzalez, C., Martin, R. L., Fox, D. J., Defrees, D. J., Baker, J. P. Stewart, J. J., and Pople, J. A., Gaussian, Pittsburgh PA, 1993.
34. Frish, M. J., Frish, A., and Foresman, J. B., *in* "Gaussian 94 User's Reference." Gaussian, Pittsburgh PA, 1995.
35. Schlegel, H. B., *in* "AB Initio Methods in Quantum Chemistry-I" (K. P. Lawley, Ed.), p. 249. Wiley, New york, 1987.
36. van Duijneveldt, F. B., van Duijneveldt-van de Rijdt, J. G. C. M., and van Lenthe, J. H., *Chem. Rev.* **94**, 1878 (1994).

37. Lendvay, G., and Mayer, I., *Chem. Phys. Lett.* **297**, 365 (1998).
38. (a) Paizs, B., and Suhai, S., *J. Comp. Chem.* **19**, 575 (1998); (b) Halász, G. J., Vibók, Á., and Mayer, I., *J. Comp. Chem.* **20**, 274 (1999).
39. Legon, A. C., and Miller, D. J., *Acc. Chem. Res.* **20**, 33 (1987).
40. van Koningsveld, H., Jansen, J. C., and van Bekkun, H., *Zeolites* **10**, 235 (1990).
41. (a) Kubelkova, L., Beran, S., and Lercher, J., A., *Zeolites* **3**, 894 (1989). (b) Brand, H. V., Curtis, L. A., and Iton, L. E., *J. Phys. Chem.* **97**, 12773 (1993); (c) Teunissen, E. H., Jansen, A. P., van Santen, R. A., and Duijnevelt, F. B., *J. Phys. Chem.* **97**, 203 (1993); (d) Kramer, G. J., and van Santen, R. A., *J. Am. Chem. Soc.* **115**, 2887 (1993); (e) Bates, S., and Dwyer, J., *J. Mol. Struct. (THEOCHEM)* **306**, 57 (1994).
42. Jänchen, J., Peeters, M. P. J., van Wolput, J. H. M. C., Wolthuizen, J. P., van Hooff, J. H. C., and Lohse, U., *J. Chem. Soc. Faraday Trans.* **90**, 1033 (1994).
43. Jänchen, J., Stach, H., Busio, M., and van Wolput, J. H. M. C., *Thermochim. Acta* **312**, 33 (1998).
44. Kuznetsov, B. V., and Tuan, N. A., Rachmanova, T. A., *Adv. Sci. Technol.* **6**, 27 (1989).
45. Kubelkova, L., Kotrla, J., and Florian, J., *J. Phys. Chem.* **99**, 10285 (1995).
46. Haw, J. F., Nicholas, J. B., Xu, T., Beck, L. W., and Ferguson, D. B., *Acc. Chem. Res.* **29**, 259 (1996).
47. (a) Barbosa, L. A. M. M., and van Santen, R. A., *J. Mol. Struct. (THEOCHEM)* **497**, 173 (2000); (b) Kazansky, V. B., and van Santen, R. A., *Catal. Lett.* **38**, 115 (1996); (c) Zhurko, D. A., Frash, M. F., and Kazansky, V. B., *Catal. Lett.* **55**, 7 (1998).
48. Barbosa, L. A. M. M., and van Santen, R. A., *J. Mol. Catal. Part A*, in press.
49. (a) Ziegler, T., *Chem. Rev.* **91**, 651(1991); (b) Wladkowski, B. D., Chenoweth, S. A., Sanders, J. N., Krauss, M., and Stevens, W. J., *J. Am. Chem. Soc.* **119**, 6423 (1997).
50. Evleth, E. M., Kassab, E., Jessri, H., Montero, L., and Sierra, L. R., *J. Phys. Chem.* **100**, 11368 (1996).
51. Tsuzuki, S., Uchimaru, T., Matsumura, K., Mikami, M., and Tanabe, K., *J. Chem. Phys.* **110**, 11906 (1999).
52. Ventura, O. N., Rama, J. B., Turi, L., and Dannenberg, J. J., *J. Phys. Chem.* **99**, 131 (1995).
53. Rak, J., Skuurski, P., Gutowski, M., Jozwiak, L., and Blaszjowsk, J., *J. Phys. Chem.* **101**, 283 (1997).
54. Cox, R. A., *J. Chem. Soc. Perkin Trans.* **2**, 1743 (1997).
55. (a) Cox, R. A., *Can. J. Chem.* **76**, 2146 (1998); (b) Cho, S. J., Lee, C. C. J. Y., Park, J. K., Suh, S. B., Park, J., Kim, B. H., and Kim, K. S., *J. Org. Chem.* **62**, 4068 (1997).
56. Kyridis, A., Cook, S. J., Chakraborty, A. K., Bell, A. T., and Theodorou, D. N., *J. Phys. Chem.* **99**, 1505 (1995).
57. Gigante, B., Santos, C., Marcelo-Curto, M. J., Coutanceau, C., Silva, J. M., Alvarez, F., Guisnet, M., Selli, E., and Forni, L., *in* "Heterogenous Catalysis and Fine Chemicals IV" (H. U. Blaser, A.Baiker, and R. Prins, Eds.), p. 547. Elsevier, Amsterdam, 1997.
58. Olah, G. A., and Kiovsky, T. E., *J. Am. Chem. Soc.* **90**, 4666 (1968).